AIMS Mathematics, 11(4): 11520–11545.
DOI: 10.3934/math.2026474
Received: 17 March 2026
Revised: 14 April 2026
Accepted: 21 April 2026
Published: 24 April 2026

https://www.aimspress.com/journal/Math

Research article

Optical solitons with polynomial law of self-phase modulation by the fourth-order conservative finite difference scheme

Jiaqi Chen[1,*], **Weizhong Dai**[2], **and Anjan Biswas**[3,4,5,6]

[1] School of Electrical Engineering and Automation, Xiamen University of Technology, Xiamen, Fujian, 361024, China

[2] Mathematics & Statistics, College of Engineering & Science, Louisiana Tech University, Ruston, LA 71272, USA

[3] Department of Mathematics and Physics, Grambling State University, Grambling, LA 71245-2715, USA

[4] Department of Mathematics, Faculty of Science, Karadeniz Technical University, Trabzon, 61080, Türkiye

[5] Department of Physics and Electronics, Khazar University, Baku, AZ-1096, Azerbaijan

[6] Department of Mathematics and Applied Mathematics, Sefako Makgatho Health Sciences University, Medunsa, Pretoria, 0204, South Africa

* **Correspondence:** Email: chenjiaqi@xmut.edu.cn.

Abstract: This paper considers an initial-boundary value problem for optical soliton propagation based on the cubic-quintic-septic nonlinear Schrödinger equation. We first analyzed the underlying physical properties of the system, formally establishing the conservation laws for mass and energy. Subsequently, we proposed a fourth-order finite difference scheme derived via the discrete variational derivative method to effectively approximate the nonlinear potential. We rigorously proved that the resulting numerical scheme perfectly satisfies the discrete analogues of the mass and energy conservation laws. Furthermore, we provided comprehensive stability and convergence analysis, demonstrating unconditional stability and establishing an error bound of $O(\tau^2 + h^4)$. Numerical experiments were conducted to validate the theoretical analysis and illustrate the efficiency and high-order accuracy of the proposed approach.

Keywords: nonlinear Schrödinger equation; finite difference method; conservation law; stability; convergence

Mathematics Subject Classification: 35Q55, 65M06, 78A60, 81V80

1. Introduction

The propagation of solitons through optical fibers, metamaterials, crystals, and various other forms of waveguides is one of the most important and successful areas of study in telecommunication engineering and quantum optics [1, 2]. One of the most commonly visible models is the nonlinear Schrödinger equation that has been widely studied and exhaustively explored mostly from an analytical perspective [3–6]. Recently, Biswas has bridged the gap by addressing the soliton cooling effect with the polynomial law of the nonlinear refractive index that is occasionally referred to as the cubic-quintic-septic law [7]. The perturbation terms considered to study the adiabatic soliton dynamics are of Hamiltonian [8] as well as non-Hamiltonian types that also include the non-local kind.

In this paper, we consider the following version of the nonlinear Schrödinger equation with the cubic-quintic-septic (polynomial) law of self-phase modulation, where the detailed initial-boundary value problem (IBVP) [9] is expressed as

$$iu_t + au_{xx} + \left[b_1|u|^2 + b_2|u|^4 + b_3|u|^6\right]u = 0, \quad (x,t) \in [x_l, x_r] \times [0,T], \tag{1.1a}$$

$$u(x,0) = \phi(x), \quad x \in [x_l, x_r], \tag{1.1b}$$

$$u(x_l,t) = u(x_r,t) = 0, \quad t \in [0,T], \tag{1.1c}$$

where $u(x,t)$ is a complex-valued function, $|u(x,t)|$ represents the moduli of this complex-valued function, and the coefficient satisfies $a > 0$. The function $\phi(x)$ represents a given smooth initial profile. The boundary conditions in Eq (1.1c) imply that the soliton is assumed to remain confined within the domain without reaching the boundaries.

All coefficients $b_k \leq 0$ (for $k = 1, 2, 3$) strictly correspond to the purely defocusing regime, which governs the propagation of dark solitons. Conversely, when all $b_k > 0$, the system is purely focusing and admits standard bright solitons. In scenarios where the coefficients b_k possess mixed signs, the system exhibits competing nonlinearities, which can support a broader and more complex class of localized structures, including flat-top and algebraic solitons [9].

Beyond traditional optical communications, solitons have found emerging applications in various advanced fields. For instance, phenomena such as physical launching mechanisms driven by cavitation have garnered recent interest [10]. In complex fiber laser systems, research has rapidly expanded into the polarization-induced buildup of soliton molecules [11, 12] and multisoliton bound states in higher-order hierarchy models [13]. Additionally, optical soliton formation has been explored in novel structures such as photonic Moiré lattices [14], alongside the observation of parton-like soliton structures in nonlinear coherent states [15]. Furthermore, soliton dynamics in partially nonlocal media have attracted significant attention, demonstrating rich physical behaviors [16, 17]. These diverse applications motivate the need for accurate and efficient numerical methods for solving nonlinear Schrödinger equations with various nonlinearity laws.

This cubic-quintic-septic form of nonlinearity has not been much studied. In [18], the author investigated and compared the variational iteration method and the residual power series method for finding numerical solutions to the cubic-quintic nonlinear Schrödinger equation. The suitability of finite difference methods and pseudo-spectral methods for validating the pulse propagation problem modeled by the nonlinear Schrödinger equation in an optical fiber were evaluated in [19]. The

objective of this study is to analyze the conservation of physical quantities, specifically mass and energy, of the above model, and then to propose a fourth-order accurate and conservative finite difference scheme to solve the IBVP.

The remainder of this paper is organized as follows. In Section 2, we analyze the conservation of physical quantities, specifically mass and energy, of the above IBVP. In Section 3, we present a fourth-order accurate and conservative finite difference scheme for solving the nonlinear Schrödinger equation with cubic-quintic-septic nonlinearity. In Section 4, we establish the discrete conservation laws of the proposed scheme and demonstrate their consistency with the continuous energy and momentum conservation laws derived in Section 2. Section 5 provides a rigorous proof of the stability and convergence of the finite difference scheme. Finally, in Section 6, we present three numerical examples to validate the accuracy and stability of the method.

2. Conservation laws

With the mathematical formulation established, we now investigate the intrinsic properties of the system. To simplify the notation, we introduce the nonlinear potential $V(s)$ defined by

$$V(s) = b_1|s|^2 + b_2|s|^4 + b_3|s|^6, \quad \forall s \in \mathbb{C}, \tag{2.1}$$

in which $|\cdot|^2$ is the square of the moduli of the complex number and we rewrite Eq (1.1a) as:

$$iu_t + au_{xx} + V(u)u = 0, \quad (x,t) \in [x_l, x_r] \times [0,T]. \tag{2.2}$$

For this nonlinear Schrödinger equation, it is essential to verify the conservation of physical quantities, specifically mass, which ensures the physical validity of the model and the stability of numerical solutions.

Proposition 2.1. *Suppose that $\phi(x) \in H_0^2[\alpha,\beta]$, and then the initial boundary value problem in Eqs (1.1a)–(1.1c) preserves the mass term $M(t)$, which is defined by*

$$M(t) = \int_{x_l}^{x_r} |u(x,t)|^2 dx.$$

Proof. To see this, we denote the conjugate part of function u to be u^*, and then we take the conjugate of Eq (1.1a). This gives

$$iu_t + au_{xx} + V(u)u = 0, \tag{2.3a}$$
$$-iu_t^* + au_{xx}^* + V(u)u^* = 0. \tag{2.3b}$$

Multiplying by the conjugate, we have:

$$iu_t u^* + au_{xx}u^* + \left[b_1|u|^2 + b_2|u|^4 + b_3|u|^6\right]|u|^2 = 0, \tag{2.4a}$$
$$-iu_t^* u + au_{xx}^* u + \left[b_1|u|^2 + b_2|u|^4 + b_3|u|^6\right]|u|^2 = 0. \tag{2.4b}$$

After subtracting, we obtain

$$(u_t u^* + u_t^* u) - ia\,(u_{xx}u^* - u_{xx}^* u) = 0, \tag{2.5}$$

which implies that

$$\frac{\partial}{\partial t}|u|^2 - ia\frac{\partial}{\partial x}\left(u_x u^* - u u_x^*\right) = 0. \tag{2.6}$$

Integrating Eq (2.6) over the domain $[x_l, x_r]$, we have

$$\frac{d}{dt}\int_{x_l}^{x_r} |u|^2 dx = ia\int_{x_l}^{x_r} \frac{\partial}{\partial x}\left(u_x u^* - u u_x^*\right) dx = ia\left(u_x u^* - u u_x^*\right)\Big|_{x_l}^{x_r} = 0, \tag{2.7}$$

by the assumption of boundary condition, and hence the result follows. □

While mass is conserved in the bounded domain with Dirichlet conditions, the conservation of momentum and energy generally requires translation invariance, which is broken by fixed boundaries. However, if we extend the problem to the entire real line, or assume the domain to be sufficiently large such that the solution and its derivatives decay to zero at infinity, the momentum is preserved. Specifically, if we assume the asymptotic boundary conditions:

$$\lim_{|x|\to\infty} u(x,t) = 0 \quad \Longrightarrow \quad \lim_{|x|\to\infty} u_x(x,t) = 0, \tag{2.8}$$

we have the following result.

Proposition 2.2. *Suppose that $\phi(x) \in H_0^2[\alpha,\beta]$, and then the initial boundary value problem in Eqs (1.1a)–(1.1c) preserves the energy term $E(t)$, which is defined by*

$$E(t) = \int_{x_l}^{x_r} \left[a|u_x(x,t)|^2 - \frac{b_1}{2}|u(x,t)|^4 - \frac{b_2}{3}|u(x,t)|^6 - \frac{b_3}{4}|u(x,t)|^8\right] dx. \tag{2.9}$$

Proof. By taking the derivative with respect to time, we have:

$$\begin{aligned}\frac{d}{dt}E(t) &= \int_{x_l}^{x_r}\left[a\frac{\partial}{\partial t}|u_x(x,t)|^2 - b_1|u|^2\frac{\partial}{\partial t}(|u|^2) - b_2|u|^4\frac{\partial}{\partial t}(|u|^2) - b_3|u|^6\frac{\partial}{\partial t}(|u|^2)\right] dx \\ &= \int_{x_l}^{x_r}\left[a\frac{\partial}{\partial t}|u_x(x,t)|^2 - V(u)\frac{\partial}{\partial t}(|u|^2)\right] dx.\end{aligned} \tag{2.10}$$

For the first term, we have:

$$\begin{aligned}\int_{x_l}^{x_r} a\frac{\partial}{\partial t}|u_x(x,t)|^2 dx &= a\int_{x_l}^{x_r}\left[u_{xt}u_x^* + u_x u_{tx}^*\right] dx \\ &= a u_t u_x^*\Big|_{x_l}^{x_r} - a\int_{x_l}^{x_r} u_t u_{xx}^* dx + a u_t^* u_x\Big|_{x_l}^{x_r} - a\int_{x_l}^{x_r} u_t^* u_{xx} dx \\ &= -a\int_{x_l}^{x_r}\left[u_t u_{xx}^* + u_t^* u_{xx}\right] dx,\end{aligned} \tag{2.11}$$

where we have applied the Neumann boundary condition. For the second term, we have:

$$\int_{x_l}^{x_r} -V(u)\frac{\partial}{\partial t}(|u|^2) dx = \int_{x_l}^{x_r} -V(u)\left(u_t u^* + u u_t^*\right) dx. \tag{2.12}$$

Combining with these results, we have:

$$\begin{aligned}\frac{d}{dt}E(t) &= -a\int_{x_l}^{x_r}\left[u_t u_{xx}^* + u_t^* u_{xx}\right]dx - \int_{x_l}^{x_r} V(u)\left(u_t u^* + u u_t^*\right)dx \\ &= -\int_{x_l}^{x_r}\left[u_t(au_{xx} + V(u)u)^* + u_t^*\left(au_{xx} + V(u)u\right)\right]dx \\ &= 0.\end{aligned} \tag{2.13}$$

The last equality is derived by simply plugging in the original partial differential equation. □

Beyond the conservation of energy, the Hamiltonian structure of the nonlinear Schrödinger equation implies the conservation of momentum. This quantity plays a critical role in the analysis of soliton stability.

Proposition 2.3. *Suppose that $\phi(x) \in H_0^2[\alpha,\beta]$, and then the initial boundary value problem in Eqs (1.1a)–(1.1c) preserves the momentum term $P(t)$, which is defined by*

$$P(t) = \int_{x_l}^{x_r} u_x(x,t)u^*(x,t)dx, \tag{2.14}$$

where $u^*(x,t)$ is the conjugate of $u(x,t)$.

Proof. To verify this property, we differentiate $P(t)$ with respect to time, and use the integration by parts for the first term and then the boundary conditions (where u_t vanishes). This gives

$$\begin{aligned}\frac{d}{dt}P(t) &= \int_{x_l}^{x_r}\left[u_{xt}u^* + u_x u_t^*\right]dx \\ &= u_t u^*\Big|_{x_l}^{x_r} + \int_{x_l}^{x_r}\left[u_x u_t^* - u_x^* u_t\right]dx \\ &= \int_{x_l}^{x_r}\left[u_x u_t^* - u_x^* u_t\right]dx.\end{aligned} \tag{2.15}$$

From the original partial differential equation, we express the time derivatives as:

$$u_t = i\left(au_{xx} + V(u)u\right), \tag{2.16a}$$

$$u_t^* = -i\left(au_{xx}^* + V(u)u^*\right). \tag{2.16b}$$

Substituting these expressions back into the integral yields:

$$\begin{aligned}\frac{d}{dt}P(t) &= \int_{x_l}^{x_r} -ia\left(u_x u_{xx}^* + u_{xx}u_x^*\right) - iV(u)\left(u_x u^* + u u_x^*\right)dx \\ &= \int_{x_l}^{x_r} -ia\frac{\partial}{\partial x}\left(|u_x|^2\right) - iV(u)\frac{\partial}{\partial x}|u|^2 dx \\ &= -ia\left(u_x u_x^*\right)\Big|_{x_l}^{x_r} - iV(u)|u|^2\Big|_{x_l}^{x_r} + i\int_{x_l}^{x_r}\frac{\partial}{\partial x}V(u)|u|^2 dx.\end{aligned} \tag{2.17}$$

The first term vanishes due to the boundary conditions ($u_x = 0$). For the second term, we recall that $V(|u|)$ is a polynomial in $|u|^2$, and therefore,

$$\int_{x_l}^{x_r} \frac{\partial}{\partial x} V(u)|u|^2 dx = \int_{x_l}^{x_r} \frac{\partial}{\partial x} \left[b_1|u|^4 + b_2|u|^6 + b_3|u|^8 \right] dx. \tag{2.18}$$

Since $u = 0$ at the boundaries, the above term also vanishes. Thus, $\frac{d}{dt}P(t) = 0$, and the result follows. □

3. Finite difference scheme

In this section, we construct a fourth-order accurate and conservative finite difference scheme for solving the IBVP in Eqs (1.1a)–(1.1c). Let J and N be positive integers, and let

$$h = \frac{x_r - x_l}{J}, \quad \tau = \frac{T}{N} \tag{3.1}$$

be the spatial and temporal step sizes, respectively. The uniform grid points are given by

$$x_j = x_l + jh, \ t^n = n\tau, \tag{3.2}$$

in which $j = 0, 1, \ldots, J$ and $n = 0, 1, \ldots, N$. Let $U_j^n \approx u(x_j, t^n)$ and denote

$$Z_h^0 = \left\{ U = (U_j) \mid U_{-2} = U_{-1} = U_{J+1} = U_{J+2} = 0 \right\}, \tag{3.3}$$

in which $-2 \le j \le J + 2$. For simplicity, we introduce the following notations:

$$\begin{aligned}
&\left(U_j^n\right)_{\tilde{x}} = \frac{U_{j+1}^n - U_j^n}{h}, \ \left(U_j^n\right)_{\bar{x}} = \frac{U_j^n - U_{j-1}^n}{h}, \ \left(U_j^n\right)_{\hat{x}} = \frac{U_{j+1}^n - U_{j-1}^n}{2h}, \\
&\left(U_j^n\right)_{\ddot{x}} = \frac{U_{j+2}^n - U_{j-2}^n}{4h}, \ \bar{U}_j^n = \frac{U_j^{n+1} + U_j^{n-1}}{2}, \ U_j^{n+\frac{1}{2}} = \frac{U_j^{n+1} + U_j^n}{2}, \\
&\left(U_j^n\right)_{\tilde{t}} = \frac{U_j^{n+1} - U_j^n}{\tau}, \ \left(U_j^n\right)_{\hat{t}} = \frac{U_j^{n+1} - U_j^{n-1}}{2\tau},
\end{aligned}$$

and we also introduce the inner product and norms defined on Z_h^0 as follows:

$$\langle U^n, V^n \rangle = h \sum_{j=1}^{J-1} U_j^n (V_j^n)^*, \ \ \|U^n\| = \sqrt{\langle U^n, U^n \rangle}, \ \ \|U^n\|_\infty = \max_{1 \le j \le J-1} |U_j^n|, \tag{3.4}$$

where $U^n, V^n \in Z_h^0$. Here, the symbols $\tilde{x}, \bar{x}, \hat{x}, \ddot{x}$ denote the forward, backward, central, and wide central spatial difference operators, respectively, and the temporal difference operators are defined in a similar manner.

We now develop a fourth-order finite difference scheme by discretizing operators and approximating all terms in Eq (1.1a).

Lemma 3.1. *(See [20, 21]) For any smooth function $u(x,t)$, it holds that:*

$$\frac{\partial u}{\partial x}(x_j,t^n)=\frac{4}{3}\Big(U_j^n\Big)_{\hat{x}}-\frac{1}{3}\Big(U_j^n\Big)_{\ddot{x}}+O(h^4), \tag{3.5a}$$

$$\frac{\partial^2 u}{\partial x^2}(x_j,t^n)=\frac{4}{3}\Big(U_j^n\Big)_{\bar{x}\bar{x}}-\frac{1}{3}\Big(U_j^n\Big)_{\hat{x}\hat{x}}+O(h^4). \tag{3.5b}$$

For the nonlinear potential term $V(u)u$, we employ the discrete variational derivative method. We first introduce the interaction potential function $H(s)$ associated with the nonlinear terms in the energy density:

$$H(s)=\frac{b_1}{2}|s|^4+\frac{b_2}{3}|s|^6+\frac{b_3}{4}|s|^8,\forall s\in\mathbb{C}. \tag{3.6}$$

Note that $V(s)=H'(s)$. With this notation, we define the following discrete potential operator Q_j^n.

Definition 3.1. *We define the discrete potential operator Q_j^n as follows:*

$$Q_j^n(U)=\begin{cases}\frac{H(U_j^{n+1})-H(U_j^{n-1})}{|U_j^{n+1}|^2-|U_j^{n-1}|^2}, & \text{if } |U_j^{n+1}|^2\neq|U_j^{n-1}|^2,\\ V(U_j^n), & \text{if } |U_j^{n+1}|^2=|U_j^{n-1}|^2.\end{cases} \tag{3.7}$$

Using the algebraic identity

$$\frac{x^k-y^k}{x-y}=\sum_{m=0}^{k-1}x^{k-1-m}y^m, \tag{3.8}$$

$Q_j^n(U)$ can be explicitly written as:

$$\begin{aligned}Q_j^n(U)=&\frac{b_1}{2}\left(|U_j^{n+1}|^2+|U_j^{n-1}|^2\right)+\frac{b_2}{3}\left(|U_j^{n+1}|^4+|U_j^{n+1}|^2|U_j^{n-1}|^2+|U_j^{n-1}|^4\right)\\&+\frac{b_3}{4}\left(|U_j^{n+1}|^6+|U_j^{n+1}|^4|U_j^{n-1}|^2+|U_j^{n+1}|^2|U_j^{n-1}|^4+|U_j^{n-1}|^6\right).\end{aligned} \tag{3.9}$$

Remark 3.1. *It should be pointed out that the idea lying in Eq (3.7) is an extension of the one in [22, 23]. Such an approximation is designed to ensure that the obtained numerical scheme satisfies the discrete analogues of both mass and energy conservation laws.*

From Lemma 3.1, we now derive a standard fourth-order accurate implicit finite difference scheme for Eqs (1.1a)–(1.1c):

$$i\Big(U_j^n\Big)_{\hat{t}}+\frac{4a}{3}\Big(\bar{U}_j^n\Big)_{\bar{x}\bar{x}}-\frac{a}{3}\Big(\bar{U}_j^n\Big)_{\hat{x}\hat{x}}+Q_j^n(U)\bar{U}_j^n=0, \tag{3.10a}$$

$$U_j^0=\phi(x_j),\ \ 0\le j\le J, \tag{3.10b}$$

$$U_0^n=U_J^n=0, \tag{3.10c}$$

where $1\le n\le N$. It should be pointed out that the boundary condition in Eq (1.1c) is replaced by $U_{-2}^n=U_{-1}^n=U_0^n=0$ for our convenience, and similarly, we assume that $U_J^n=U_{J+1}^n=U_{J+2}^n=0$, where $j=-2,-1,J+1,J+2$ are ghost grid points for all $1\le n\le N$, indicating that $U^n\in Z_h^0$.

This boundary condition at ghost grid points is reasonable since we simulate the soliton propagation and we assume that the soliton never reaches the boundary. Since the fourth-order compact difference

scheme only involves spatial operators up to second order, setting two additional ghost points to zero is consistent with the smooth extension of the solution beyond the boundary. Specifically, the Taylor expansion of the exact solution near $x = x_l$ gives

$$u(x_l - h, t) = u(x_l, t) - hu_x(x_l, t) + O(h^2), \tag{3.11}$$

and similarly for $x_l - 2h$, ensuring no boundary artifacts are introduced to the $O(h^4)$ accuracy of the scheme.

To initiate our finite difference scheme, we consider the following two-level, fourth-order accurate difference scheme for U^1:

$$i\left(U_j^0\right)_{\tilde{t}} + \frac{4a}{3}\left(U_j^{\frac{1}{2}}\right)_{\tilde{x}\bar{x}} - \frac{a}{3}\left(U_j^{\frac{1}{2}}\right)_{\hat{x}\hat{x}} + \left[\frac{H(U_j^1) - H(U_j^0)}{|U_j^1|^2 - |U_j^0|^2}\right]\left(U_j^{\frac{1}{2}}\right) = 0, \tag{3.12}$$

where $U^{\frac{1}{2}} = \left(U^1 + U^0\right)/2$.

4. Discrete conservation laws

In this section, we derive the conservation laws for the finite difference scheme Eqs (3.10a)–(3.10c) and (3.12) proposed in the previous section. To facilitate the subsequent analysis, we begin by recalling several fundamental algebraic properties and inequality estimates for discrete mesh functions.

First, the following lemma summarizes essential summation-by-parts formulas and inner product identities.

Lemma 4.1. *(See [24]) For any two mesh functions $U, V \in Z_h^0$, it holds that:*

$$\begin{aligned}
&\langle U_{\hat{x}}, V\rangle = -\langle U, V_{\hat{x}}\rangle,\ \langle U_{\ddot{x}}, V\rangle = -\langle U, V_{\ddot{x}}\rangle,\\
&\mathfrak{R}\left\{\langle U_{\hat{x}}, U\rangle\right\} = 0,\ \mathfrak{R}\left\{\langle U_{\ddot{x}}, U\rangle\right\} = 0,\\
&\langle U_{\tilde{x}\bar{x}}, U\rangle = -\|U_{\hat{x}}\|^2,\ \langle U_{\hat{x}\hat{x}}, U\rangle = -\|U_{\hat{x}}\|^2,
\end{aligned}$$

where $\mathfrak{R}$ denotes the real part of the complex number.

Next, we establish the ordering relations among the norms of various difference operators.

Lemma 4.2. *(See [24]) For any mesh function $U \in Z_h^0$, we have:*

$$\|U_{\ddot{x}}^n\| \le \|U_{\hat{x}}^n\| \le \|U_{\tilde{x}}^n\| = \|U_{\bar{x}}^n\|.$$

Lemma 4.3. *(See [24]) For any mesh function $U \in Z_h^0$, there exists positive constants $C_1, C_2 > 0$, which are independent of h and τ but depend on the length of domain $L = x_r - x_l$, such that*

$$\|U^n\| \le C_1\|U_{\tilde{x}}^n\|, \quad \|U^n\|_\infty \le C_2\|U_{\tilde{x}}^n\|,$$

where $C_1 = \frac{L}{\sqrt{6}}$ and $C_2 = \frac{L}{\sqrt{2}}$ are optimal.

With these auxiliary results, we are now positioned to derive the discrete mass and energy conservation laws.

Proposition 4.1. *Suppose mesh function $U^n \in Z_h^0$, and then the difference scheme we proposed in Eqs (3.10a)–(3.10c) and (3.12) conserves the following discrete invariant:*

$$M^n = \frac{1}{2}\left(\left\|U^{n+1}\right\|^2 + \|U^n\|^2\right). \tag{4.1}$$

Proof. By multiplying $\left(\bar{U}_j^n\right)^*$ to the difference scheme Eq (3.10a), summing over index j, and then choosing the imaginary part, we have:

$$i\sum_{j=1}^{J-1}\left(U_j^n\right)_{\hat{t}}\left(\bar{U}_j^n\right)^* + \frac{4a}{3}\sum_{j=1}^{J-1}\left(\bar{U}_j^n\right)_{\tilde{x}\tilde{x}}\left(\bar{U}_j^n\right)^* - \frac{a}{3}\sum_{j=1}^{J-1}\left(\bar{U}_j^n\right)_{\hat{x}\hat{x}}\left(\bar{U}_j^n\right)^* + \sum_{j=1}^{J-1} Q_j^n(U)\bar{U}_j^n\left(\bar{U}_j^n\right)^* = 0. \tag{4.2}$$

For the first term,

$$\Im\left\{i\sum_{j=1}^{J-1}\left(U_j^n\right)_{\hat{t}}\left(\bar{U}_j^n\right)^*\right\} = \frac{i}{4\tau}\left(\left\|U^{n+1}\right\|^2 - \left\|U^{n-1}\right\|^2\right), \tag{4.3}$$

which is purely imaginary. For the second and third terms, we have:

$$\frac{4a}{3}\sum_{j=1}^{J-1}\left(\bar{U}_j^n\right)_{\tilde{x}\tilde{x}}\left(\bar{U}_j^n\right)^* - \frac{a}{3}\sum_{j=1}^{J-1}\left(\bar{U}_j^n\right)_{\hat{x}\hat{x}}\left(\bar{U}_j^n\right)^* = -\frac{4a}{3}\left(\left\|\bar{U}_{\hat{x}}^n\right\|^2\right) + \frac{a}{3}\left(\left\|\bar{U}_{\hat{x}}^n\right\|^2\right) = -a\left\|\bar{U}_{\hat{x}}^n\right\|^2, \tag{4.4}$$

which is purely real. For the nonlinear term, we have:

$$Q_j^n(U)\bar{U}_j^n\left(\bar{U}_j^n\right)^* = Q_j^n(U)\left|\bar{U}_j^n\right|^2, \tag{4.5}$$

which is also purely real. Now for the imaginary part, we have:

$$\left\|U^{n+1}\right\|^2 - \left\|U^{n-1}\right\|^2 = 0, \tag{4.6}$$

which implies that

$$M^n := \frac{1}{2}\left(\left\|U^{n+1}\right\|^2 + \|U^n\|^2\right) = M^{n-1} = \cdots = M^1. \tag{4.7}$$

For the initial step, multiplying Eq (3.12) by $\left(U_j^{\frac{1}{2}}\right)^*$, summing over all indices, and taking the imaginary part, we obtain

$$\|U^1\|^2 - \|U^0\|^2 = 0, \tag{4.8}$$

and we simply define $M^0 = \frac{1}{2}\left(\|U^1\|^2 + \|U^0\|^2\right)$. Then the result follows. □

Proposition 4.2. *Suppose $U^n \in Z_h^0$, and then the difference scheme we proposed in Eqs (3.10a)–(3.10c) and (3.12) conserves the following discrete invariant $E^n = E^{n-1} = \cdots = E^1 = E^0$, where*

$$E^n = \frac{a}{2}\left(\|U_{\hat{x}}^{n+1}\|^2 + \|U_{\hat{x}}^n\|^2\right) + \frac{1}{2}\left(H(U^{n+1}) + H(U^n)\right). \tag{4.9}$$

Proof. Instead of multiplying $\left(\bar{U}_j^n\right)^*$, we multiply the finite difference scheme, Eq (3.10a), by $(U_j^{n+1} - U_j^{n-1})^*$ and sum over the spatial grid points. Taking the real part of the resulting equation, the term involving time differentiation and linear spatial operators yields the change in kinetic energy.

The first term becomes:

$$i\sum_{j=1}^{J-1}\left(U_j^n\right)_{\hat{t}}\left(U_j^{n+1} - U_j^{n-1}\right)^* = i\sum_{j=1}^{J-1}\|U_j^{n+1} - U_j^{n-1}\|^2, \tag{4.10}$$

which contains only an imaginary term. For the spatial difference terms, we have:

$$\begin{aligned}
&\sum_{j=1}^{J-1}\left(\frac{4a}{3}\left(\bar{U}_j^n\right)_{\bar{x}\bar{x}} - \frac{a}{3}\left(\bar{U}_j^n\right)_{\hat{x}\hat{x}}\right)\left(U_j^{n+1} - U_j^{n-1}\right)^* \\
&= \frac{2a}{3}\sum_{j=1}^{J-1}\left(\left|\left(U_j^{n+1}\right)_{\hat{x}}\right|^2 - \left|\left(U_j^{n-1}\right)_{\hat{x}}\right|^2\right) - \frac{a}{6}\sum_{j=1}^{J-1}\left(\left|\left(U_j^{n+1}\right)_{\hat{x}}\right|^2 - \left|\left(U_j^{n-1}\right)_{\hat{x}}\right|^2\right) \\
&= \frac{a}{2}\left(\|U_{\hat{x}}^{n+1}\|^2 - \|U_{\hat{x}}^{n-1}\|^2\right).
\end{aligned} \tag{4.11}$$

For the nonlinear term, if $|U_j^{n+1}|^2 = |U_j^{n-1}|^2$, then $Q_j^n(U) = V(U_j^n)$ and hence

$$Q_j^n(U)\bar{U}_j^n\left(U_j^{n+1} - U_j^{n-1}\right)^* = V(U_j^n)(|U_j^{n+1}|^2 - |U_j^{n-1}|^2) = 0. \tag{4.12}$$

Therefore, the nonlinear term becomes:

$$\begin{aligned}
\sum_{j=1}^{J-1} Q_j^n(U)\bar{U}_j^n\left(U_j^{n+1} - U_j^{n-1}\right)^* &= \frac{1}{2}\sum_{j=1}^{J-1} Q_j^n(U)\left(\left|U_j^{n+1}\right|^2 - \left|U_j^{n-1}\right|^2\right) \\
&= \frac{1}{2}\sum_{j=1}^{J-1}\left(H(U_j^{n+1}) - H(U_j^{n-1})\right) \\
&= \frac{1}{2}\left(H(U^{n+1}) - H(U^{n-1})\right),
\end{aligned} \tag{4.13}$$

by the definitions of $Q_j^n(U)$ and $H(\cdot)$ that we defined in Eqs (3.6) and (3.7). Summing over all grid points and utilizing the telescoping sum property, we arrive at the conservation law. For the initial step, multiplying Eq (3.12) by $(U_j^1 - U_j^0)^*$, and taking the real part, the result follows by a similar argument. □

Remark 4.1. *Combining Propositions 4.1 and 4.2 with Lemmas 4.2 and 4.3, we establish that the mesh function U^n is bounded in the discrete H_0^2-norm. Consequently, the discrete Sobolev embedding implies that U^n is also bounded in the L^∞-norm, a property that is crucial for the analysis in the next section.*

5. Stability and convergence

In this section, we examine the stability and convergence of the finite difference scheme in Eqs (3.10a)–(3.10c) and (3.12). We start with two lemmas about the Sobolev embedding theorem and the boundedness of functions.

Lemma 5.1. *Let $\Omega \subset \mathbb{R}$ be a bounded interval. Then, the Sobolev space $H^1(\Omega)$ is continuously embedded into the space of bounded continuous functions, i.e., $H^1(\Omega) \hookrightarrow L^\infty(\Omega)$. Furthermore, since Ω has finite measure ($|\Omega| < \infty$), the $L^p(\Omega)$ spaces are nested. Specifically, for any $1 \le q < p \le \infty$, we have the continuous embedding $L^p(\Omega) \hookrightarrow L^q(\Omega)$. Consequently, the following chain of embeddings holds:*

$$H^1(\Omega) \hookrightarrow L^\infty(\Omega) \hookrightarrow L^8(\Omega) \hookrightarrow L^6(\Omega) \hookrightarrow L^4(\Omega) \hookrightarrow L^2(\Omega). \tag{5.1}$$

The standard proof can be found in various textbooks about partial differential equations, and we refer the reader to [25].

Lemma 5.2. *Assume that the initial data $\phi \in H_0^2(\Omega)$ and that the constants satisfy $a > 0$. Then, the solution u^n of the initial boundary value problem Eqs (1.1a)–(1.1c) satisfies the uniform estimates*

$$\|u^n\|_{L^2(\Omega)} \le C, \quad \|u_x^n\|_{L^2(\Omega)} \le C, \quad \text{and} \quad \|u^n\|_{L^\infty(\Omega)} \le C, \tag{5.2}$$

where $C > 0$ is a constant depending on the initial data ϕ, the domain size $|\Omega|$, and the parameters a, b_1, b_2, b_3, but independent of the mesh sizes h and τ.

Proof. Applying the conservation of mass and energy in Propositions 2.1 and 2.2 yields

$$\|u^n\|_{L^2(\Omega)} \le \|\phi\|_{L^2(\Omega)} \tag{5.3}$$

and

$$\|u_x^n\|_{L^2(\Omega)}^2 \le \frac{E(0)}{a}, \tag{5.4}$$

where the initial energy $E(0)$ is defined as

$$E(0) = \int_{x_l}^{x_r} \left[a|\phi_x|^2 - \frac{b_1}{2}|\phi|^4 - \frac{b_2}{3}|\phi|^6 - \frac{b_3}{4}|\phi|^8 \right] dx. \tag{5.5}$$

Since Ω is a bounded domain, we have the continuous embeddings $L^8(\Omega) \hookrightarrow L^6(\Omega) \hookrightarrow L^4(\Omega) \hookrightarrow L^2(\Omega)$. Given $\phi \in H_0^2(\Omega)$, it follows that $\phi \in L^8(\Omega)$ and $\phi_x \in L^2(\Omega)$, thus, $E(0)$ is bounded.

Finally, the Sobolev embedding theorem in one dimension, $H^1(\Omega) \hookrightarrow L^\infty(\Omega)$, implies

$$\|u^n\|_{L^\infty(\Omega)} \le C_\Omega \|u^n\|_{H^1(\Omega)} \le C_\Omega \left(\|u^n\|_{L^2(\Omega)} + \|u_x^n\|_{L^2(\Omega)} \right). \tag{5.6}$$

Combining these estimates completes the proof. □

Before we state the boundedness theorem for the error term, we introduce the following lemma for the functional $Q_j^n(U)$ that we defined in our difference scheme. By the definition in Eq (3.9), $Q_j^n(U)$ can be explicitly written as:

$$\begin{aligned} Q_j^n(U) = {} & \frac{b_1}{2}\left(|U_j^{n+1}|^2 + |U_j^{n-1}|^2 \right) + \frac{b_2}{3}\left(|U_j^{n+1}|^4 + |U_j^{n+1}|^2 |U_j^{n-1}|^2 + |U_j^{n-1}|^4 \right) \\ & + \frac{b_3}{4}\left(|U_j^{n+1}|^6 + |U_j^{n+1}|^4 |U_j^{n-1}|^2 + |U_j^{n+1}|^2 |U_j^{n-1}|^4 + |U_j^{n-1}|^6 \right), \end{aligned} \tag{5.7}$$

in which we can see that $Q_j^n(U)$ in fact depends on both U_j^{n+1} and U_j^{n-1}. Now we define the following functional:

$$Q(u, v) = \frac{b_1}{2}\left(|u|^2 + |v|^2 \right) + \frac{b_2}{3}\left(|u|^4 + |u|^2|v|^2 + |v|^4 \right) + \frac{b_3}{4}\left(|u|^6 + |u|^4|v|^2 + |u|^2|v|^4 + |v|^6 \right). \tag{5.8}$$

With this definition, $Q_j^n(U) = Q(U_j^{n+1}, U_j^{n-1})$ and we have the following lemma.

Lemma 5.3. *The functional*

$$Q : L^\infty(\Omega) \times L^\infty(\Omega) \to \mathbb{R} \tag{5.9}$$

is Lipschitz continuous, that is, assume that $u_1, u_2, v_1, v_2 \in L^\infty(\Omega)$, where $\Omega = [x_l, x_r] \subset \mathbb{R}$, and then

$$|Q(u_1, v_1) - Q(u_2, v_2)| \leq C\left(|u_1 - u_2| + |v_1 - v_2|\right), \tag{5.10}$$

where C is a constant depending on the L^∞-norms $\|u_1\|_{L^\infty(\Omega)}$, $\|u_2\|_{L^\infty(\Omega)}$, $\|v_1\|_{L^\infty(\Omega)}$, $\|v_2\|_{L^\infty(\Omega)}$ and the coefficients b_1, b_2, b_3.

Proof. Assume the mesh functions are bounded in the discrete L^∞-norm. That is, there exists a constant $M > 0$ such that

$$\|u_1\|_{L^\infty(\Omega)}, \|u_2\|_{L^\infty(\Omega)}, \|v_1\|_{L^\infty(\Omega)}, \|v_2\|_{L^\infty(\Omega)} \leq M. \tag{5.11}$$

To prove the Lipschitz continuity, we analyze the variation of each term in Q with respect to the boundedness assumption. We utilize the fundamental inequality for powers:

$$\left||a|^k - |b|^k\right| \leq kM^{k-1}|a - b|, \quad \text{for } |a|, |b| \leq M. \tag{5.12}$$

First, we consider the quadratic term associated with b_1. Using the triangle inequality and the bound M, we have:

$$\left||u_1|^2 - |u_2|^2\right| = |(|u_1| - |u_2|)(|u_1| + |u_2|)| \leq 2M|u_1 - u_2|. \tag{5.13}$$

A similar estimate holds for the $|v|^2$ term.

Next, we examine the quartic terms associated with b_2. The pure power terms $|u_1|^4 - |u_2|^4$ and $|v_1|^4 - |v_2|^4$ are bounded by $4M^3|u_1 - u_2|$ and $4M^3|v_1 - v_2|$, respectively. For the mixed term $|u|^2|v|^2$, we apply the technique of adding and subtracting $|u_2|^2|v_1|^2$:

$$\begin{aligned}
\left||u_1|^2|v_1|^2 - |u_2|^2|v_2|^2\right| &= \left||u_1|^2|v_1|^2 - |u_2|^2|v_1|^2 + |u_2|^2|v_1|^2 - |u_2|^2|v_2|^2\right| \\
&\leq |v_1|^2\left||u_1|^2 - |u_2|^2\right| + |u_2|^2\left||v_1|^2 - |v_2|^2\right| \\
&\leq M^2(2M|u_1 - u_2|) + M^2(2M|v_1 - v_2|) \\
&= 2M^3\left(|u_1 - u_2| + |v_1 - v_2|\right).
\end{aligned} \tag{5.14}$$

Finally, for the sextic terms associated with b_3, we apply the same argument. The term $|u|^6$ yields a Lipschitz constant of $6M^5$. The mixed terms, such as $|u|^4|v|^2$, can be bounded by:

$$\left||u_1|^4|v_1|^2 - |u_2|^4|v_2|^2\right| \leq 4M^5|u_1 - u_2| + 2M^5|v_1 - v_2|. \tag{5.15}$$

Summing the contributions from all terms, we obtain a global Lipschitz constant C of the form:

$$C = C_1|b_1|M + C_2|b_2|M^3 + C_3|b_3|M^5, \tag{5.16}$$

where C_1, C_2, C_3 are positive constants. This concludes the proof. □

Remark 5.1. *We note that the grid functions u and v are complex-valued. However, the functional Q depends exclusively on the moduli of these functions. The proof remains valid in the complex case by invoking the reverse triangle inequality, $\left||z_1| - |z_2|\right| \leq |z_1 - z_2|$ for any $z_1, z_2 \in \mathbb{C}$. Consequently, the estimates for the differences of powers, such as $\left||u_1|^k - |u_2|^k\right|$, are bounded by the modulus of the difference $|u_1 - u_2|$, preserving the Lipschitz property for complex functions.*

We now proceed to establish the convergence property. Before stating the theorem, we provide a brief remark on the regularity assumption of the exact solution.

Remark 5.2. *The subsequent convergence analysis requires the exact solution to possess sufficient smoothness, specifically $u \in C^{2,1}_{x,t}([x_l, x_r] \times [0, T])$. For the generalized nonlinear Schrödinger equation with high-order polynomial nonlinearities, standard well-posedness theory dictates that if the initial data $\phi(x)$ is sufficiently smooth (e.g., $\phi \in H^s(\Omega)$ for $s \geq 2$) and the parameters reside in a regime that avoids finite-time blow-up, the solution maintains this required regularity throughout the domain. Detailed analytical proofs for these regularity properties can be found in the comprehensive literature on semilinear Schrödinger equations [3].*

Proposition 5.1. *Assume that the initial data $\phi \in H^2_0(\Omega)$ and that the constants satisfy $a > 0$. We further assume that the solution u^n of the initial boundary value problem in Eqs (1.1a)–(1.1c) satisfies $u^n \in C^{2,1}_{x,t}([x_l, x_r] \times [0, T])$. It can be concluded that the solution U^n of the difference scheme in Eqs (3.10a)–(3.10c) and (3.12) converges to the solution u^n and the rate of convergence is $O(\tau^2 + h^4)$.*

Proof. The truncation errors of Eqs (1.1a)–(1.1c) can be written as:

$$r_j^n = i\left(u_j^n\right)_{\hat{t}} + \frac{4a}{3}\left(\bar{u}_j^n\right)_{\bar{x}\bar{x}} - \frac{a}{3}\left(\bar{u}_j^n\right)_{\hat{x}\hat{x}} + Q_j^n(u)\bar{u}_j^n, \tag{5.17a}$$

$$u_j^0 = \phi(x_j), \quad 0 \leq j \leq J, \tag{5.17b}$$

$$u_0^n = u_J^n = 0. \tag{5.17c}$$

By the Taylor expansion, $|r_j^n| \leq O(\tau^2 + h^4)$ as the mesh constants $\tau, h \to 0$ for $n > 0$.

Let $e_j^n = u_j^n - U_j^n$. Combining with the difference scheme in Eqs (3.10a)–(3.10c) and (3.12), we obtain:

$$r_j^n = i\left(e_j^n\right)_{\hat{t}} + \frac{4a}{3}\left(\bar{e}_j^n\right)_{\bar{x}\bar{x}} - \frac{a}{3}\left(\bar{e}_j^n\right)_{\hat{x}\hat{x}} + Q_j^n(u)\bar{u}_j^n - Q_j^n(U)\bar{U}_j^n, \tag{5.18a}$$

$$e_j^0 = 0, \quad 0 \leq j \leq J, \tag{5.18b}$$

$$e_0^n = e_J^n = 0. \tag{5.18c}$$

Multiplying Eq (5.18a) by $(\bar{e}_j^n)^*$ and mesh constant h, and summing over all indices, for the right-hand side, the imaginary part of the first term is

$$\Im\left\{ih\sum_{j=1}^{J-1}\left(e_j^n\right)_{\hat{t}} \cdot (\bar{e}_j^n)^*\right\} = \frac{1}{4\tau}\left(\|e^{n+1}\|^2 - \|e^{n-1}\|^2\right). \tag{5.19}$$

For the second-order term, we have:

$$\frac{4ah}{3}\sum_{j=1}^{J-1}\left(\bar{e}_j^n\right)_{\bar{x}\bar{x}}\left(\bar{e}_j^n\right)^* - \frac{ah}{3}\sum_{j=1}^{J-1}\left(\bar{e}_j^n\right)_{\hat{x}\hat{x}}\left(\bar{e}_j^n\right)^* = -\frac{4ah}{3}\left(\left\|\bar{e}_{\hat{x}}^n\right\|^2\right) + \frac{ah}{3}\left(\left\|\bar{e}_{\hat{x}}^n\right\|^2\right), \tag{5.20}$$

which is a purely real value. For the nonlinear term, we first apply the technique of adding and subtracting:

$$\begin{aligned} Q_j^n(u)\bar{u}_j^n - Q_j^n(U)\bar{U}_j^n &= Q_j^n(u)\bar{u}_j^n - Q_j^n(u)\bar{U}_j^n + Q_j^n(u)\bar{U}_j^n - Q_j^n(U)\bar{U}_j^n \\ &= Q_j^n(u)\bar{e}_j^n + \left(Q_j^n(u) - Q_j^n(U)\right)\bar{U}_j^n \\ &= Q_j^n(u)\bar{e}_j^n + \left(\mathcal{Q}(u_j^{n+1}, u_j^{n-1}) - \mathcal{Q}(U_j^{n+1}, U_j^{n-1})\right)\bar{U}_j^n. \end{aligned} \tag{5.21}$$

After multplying Eq (5.21) by $(\bar{e}_j^n)^*$ and h, and taking the imaginary part, we have:

$$\begin{aligned}
&\Im\left\{h\sum_{j=1}^{J-1}\left(Q_j^n(u)\bar{u}_j^n - Q_j^n(U)\bar{U}_j^n\right)(\bar{e}_j^n)^*\right\}\\
&= \Im\left\{h\sum_{j=1}^{J-1}Q_j^n(u)|\bar{e}_j^n|^2 + h\sum_{j=1}^{J-1}\left(Q(u_j^{n+1},u_j^{n-1}) - Q(U_j^{n+1},U_j^{n-1})\right)\bar{U}_j^n(\bar{e}_j^n)^*\right\}\\
&= \Im\left\{h\sum_{j=1}^{J-1}\left(Q(u_j^{n+1},u_j^{n-1}) - Q(U_j^{n+1},U_j^{n-1})\right)\bar{U}_j^n(\bar{e}_j^n)^*\right\},
\end{aligned} \tag{5.22}$$

since the first term is a purely real value. Thus, the error equation reduces to:

$$\Im\left\{h\sum_{j=1}^{J-1}r_j^n(\bar{e}_j^n)^*\right\} = \frac{\|e^{n+1}\|^2 - \|e^{n-1}\|^2}{4\tau} + \Im\left\{h\sum_{j=1}^{J-1}\left(Q(u_j^{n+1},u_j^{n-1}) - Q(U_j^{n+1},U_j^{n-1})\right)\bar{U}_j^n(\bar{e}_j^n)^*\right\}, \tag{5.23}$$

and it satisfies:

$$\frac{\|e^{n+1}\|^2 - \|e^{n-1}\|^2}{4\tau} \le \left|\Im\left\{h\sum_{j=1}^{J-1}\left(Q(u_j^{n+1},u_j^{n-1}) - Q(U_j^{n+1},U_j^{n-1})\right)\bar{U}_j^n(\bar{e}_j^n)^*\right\}\right| + \left|\Im\left\{h\sum_{j=1}^{J-1}r_j^n(\bar{e}_j^n)^*\right\}\right|. \tag{5.24}$$

Based on the Lipschitz continuity of Q and Remark 4.1 (i.e., the numerical solution is bounded, $\|U^n\|_\infty \le M$ for some constant M), there exists a constant C_1 such that:

$$\left|Q(u_j^{n+1},u_j^{n-1}) - Q(U_j^{n+1},U_j^{n-1})\right| \le C_1\left(|e_j^{n+1}| + |e_j^{n-1}|\right). \tag{5.25}$$

Substituting this into the first term gives

$$\begin{aligned}
\left|h\sum_{j=1}^{J-1}\left(Q(u_j^{n+1},u_j^{n-1}) - Q(U_j^{n+1},U_j^{n-1})\right)\bar{U}_j^n(\bar{e}_j^n)^*\right| &\le h\sum_{j=1}^{J-1}C_1\left(|e_j^{n+1}| + |e_j^{n-1}|\right)M|\bar{e}_j^n|\\
&\le C_2 h\sum_{j=1}^{J-1}\left(|e_j^{n+1}| + |e_j^{n-1}|\right)^2\\
&\le C\left(\|e^{n+1}\|^2 + \|e^{n-1}\|^2\right),
\end{aligned} \tag{5.26}$$

where C is a generic positive constant independent of τ and h. By using the Cauchy-Schwarz inequality and Young's inequality:

$$\left|h\sum_{j=1}^{J-1}r_j^n(\bar{e}_j^n)^*\right| \le \|r^n\|\|\bar{e}^n\| \le \frac{1}{2}\|r^n\|^2 + \frac{1}{2}\|\bar{e}^n\|^2 \le \frac{1}{2}\|r^n\|^2 + C\left(\|e^{n+1}\|^2 + \|e^{n-1}\|^2\right). \tag{5.27}$$

Substituting these estimates back into Eq (5.24) yields:

$$\frac{\|e^{n+1}\|^2 - \|e^{n-1}\|^2}{4\tau} \le C\left(\|e^{n+1}\|^2 + \|e^{n-1}\|^2\right) + \frac{1}{2}\|r^n\|^2. \tag{5.28}$$

Multiplying by 4τ and rearranging terms:

$$(1 - 4\tau C)\|e^{n+1}\|^2 \leq (1 + 4\tau C)\|e^{n-1}\|^2 + 2\tau\|r^n\|^2. \tag{5.29}$$

For sufficiently small τ such that $1 - 4\tau C > 0$, we have:

$$\|e^{n+1}\|^2 \leq \left(\frac{1 + 4\tau C}{1 - 4\tau C}\right)\|e^{n-1}\|^2 + \frac{2\tau}{1 - 4\tau C}\|r^n\|^2. \tag{5.30}$$

We obtain:

$$\|e^{n+1}\|^2 \leq (1 + C'\tau)\|e^{n-1}\|^2 + C'\tau\|r^n\|^2 \tag{5.31}$$

for some constant C'. Let $E^n = \|e^n\|^2$. Applying the discrete Grönwall inequality [26, 27], and noting that $E^0 = 0$, we have

$$\|e^n\|^2 \leq \exp(C'T)\left(\tau \sum_{k=1}^{n} \|r^k\|^2\right). \tag{5.32}$$

Since the truncation error is bounded by $\|r^k\| = O(\tau^2 + h^4)$, the sum is bounded by:

$$\tau \sum_{k=1}^{n} \|r^k\|^2 \leq T \cdot \max_{1\leq k\leq N} \|r^k\|^2 \leq CT(\tau^2 + h^4)^2. \tag{5.33}$$

Therefore, taking the square root, we obtain the convergence rate:

$$\|e^n\| \leq C(\tau^2 + h^4). \tag{5.34}$$

This completes the proof. □

6. Numerical experiments

In this section, we present numerical results to verify the theoretical analysis and to demonstrate the efficiency of the proposed difference scheme. We perform simulations across three distinct examples to test the scheme's order of accuracy and its ability to preserve discrete mass and energy. Example 1 focuses on a case with an exact solution to establish error bounds, while Examples 2 and 3 explore more complex scenarios.

6.1. Implementation details

The computational procedure is presented as follows:

- Step 1: U^0 is obtained by the proposed initial conditions.
- Step 2: To initiate our scheme, we first solve U^1 based on Eq (3.12). Since there exists a nonlinear term in the scheme, we present an iterative algorithm:

$$\begin{aligned} \frac{i}{\tau}\left(U_j^{1(m+1)} - U_j^0\right) + \frac{4a}{3}\left(U_j^{1(m+1)} + U_j^0\right)_{\bar{x}\bar{x}} - \frac{a}{3}\left(U_j^{1(m+1)} + U_j^0\right)_{\hat{x}\hat{x}} \\ + \frac{1}{2}\left[\frac{H(U_j^{1(m)}) - H(U_j^0)}{|U_j^{1(m)}|^2 - |U_j^0|^2}\right]\left(U_j^{1(m+1)} + U_j^0\right) = 0, \end{aligned} \tag{6.1}$$

  in which $m = 1, 2, \ldots$, with the initial iterative value $U_j^{1(0)} = U_j^0$. The iterative procedure will be terminated if $\|U_j^{1(m+1)} - U_j^{1(m)}\| \leq 10^{-10}$.

- Step 3: For U^{n+1}, we use Eqs (3.10a)–(3.10c) and present an iterative algorithm:

$$\frac{i}{2\tau}\left(U_j^{n+1(m+1)}-U_j^{n-1}\right)+\frac{4a}{3}\left(U_j^{n+1(m+1)}+U_j^{n-1}\right)_{\bar{x}\bar{x}}-\frac{a}{3}\left(U_j^{n+1(m+1)}+U_j^{n-1}\right)_{\hat{x}\hat{x}} + \frac{1}{2}Q_j^n(U)\left(U_j^{n+1(m+1)}+U_j^{n-1}\right)=0, \tag{6.2}$$

in which the function Q is defined in Eq (3.9) as follows:

$$Q_j^n(U)=\frac{b_1}{2}\left(|U_j^{n+1(m)}|^2+|U_j^{n-1}|^2\right)+\frac{b_2}{3}\left(|U_j^{n+1(m)}|^4+|U_j^{n+1(m)}|^2|U_j^{n-1}|^2+|U_j^{n-1}|^4\right) + \frac{b_3}{4}\left(|U_j^{n+1(m)}|^6+|U_j^{n+1(m)}|^4|U_j^{n-1}|^2+|U_j^{n+1(m)}|^2|U_j^{n-1}|^4+|U_j^{n-1}|^6\right) \tag{6.3}$$

in which $m=1,2,\ldots$, with the initial iterative value $U_j^{n+1(0)}=U_j^n$. The iterative procedure will be terminated if $\|U_j^{n+1(m+1)}-U_j^{n+1(m)}\|\le 10^{-10}$.

We remark that both linear systems we apply have a penta-diagonal structure and can be solved efficiently by the Thomas algorithm.

6.2. Error norms and convergence rates

To evaluate the accuracy of our difference scheme, we consider two cases depending on the availability of the exact solution.

If the exact solution u is provided, to quantify the accuracy, we define the error between the numerical solution u^n and the exact solution $u(x,t_n)$ using the standard discrete L_2-norm and L_∞-norm, denoted by $\|e^n\|_2$ and $\|e^n\|_\infty$, respectively.

$$\|e^n\|_2=\left[h\sum_{j=1}^{J-1}|u_j^n-U_j^n|^2\right]^{\frac{1}{2}},\quad \|e^n\|_\infty=\max_{1\le j\le J-1}|u_j^n-U_j^n|. \tag{6.4}$$

Assuming a scaling where the time step reduces quadratically with the spatial step ($\tau\propto h^2$), the rates of convergence in the spatial direction are computed as:

$$r_{h,2}=\log_2\left(\frac{\|e^n(h,\tau)\|_2}{\|e^n(h/2,\tau/4)\|_2}\right),\quad r_{h,\infty}=\log_2\left(\frac{\|e^n(h,\tau)\|_\infty}{\|e^n(h/2,\tau/4)\|_\infty}\right). \tag{6.5}$$

Similarly, for a sufficiently small spatial step h, the rates of convergence in the temporal direction are defined as:

$$r_{\tau,2}=\log_2\left(\frac{\|e^n(h,\tau)\|_2}{\|e^n(h,\tau/2)\|_2}\right),\quad r_{\tau,\infty}=\log_2\left(\frac{\|e^n(h,\tau)\|_\infty}{\|e^n(h,\tau/2)\|_\infty}\right). \tag{6.6}$$

In the absence of an exact analytical solution, we assess the numerical accuracy and convergence order using the following Cauchy error principle. We define the spatial Cauchy error norms as:

$$\|E^n(h,\tau)\|_2=\left[h\sum_{j=1}^{J-1}\left|U_j^n(h,\tau)-U_{2j}^n(h/2,\tau)\right|^2\right]^{\frac{1}{2}}, \tag{6.7a}$$

$$\|E^n(h,\tau)\|_\infty = \max_{1\le j\le J-1} \left|U_j^n(h,\tau) - U_{2j}^n(h/2,\tau)\right|. \tag{6.7b}$$

Note that the solution on the fine mesh, denoted by grid spacing $h/2$, is restricted to the coarse mesh points via the index $2j$.

$$r_{\tau,2} = \log_2\left(\frac{\|E^n(h,\tau)\|_2}{\|E^n(h/2,\tau)\|_2}\right), \quad r_{\tau,\infty} = \log_2\left(\frac{\|E^n(h,\tau)\|_\infty}{\|E^n(h/2,\tau)\|_\infty}\right). \tag{6.8}$$

6.3. Example 1

To validate the theoretical analysis and demonstrate the efficiency of the proposed difference scheme, we first verify the error bounds using a case where an exact solution is available. By isolating the high-order nonlinearity, we can rigorously test the scheme's ability to maintain high-order accuracy and conservation properties in the presence of strong nonlinear effects.

By setting $b_1 = b_2 = 0$, the original equation reduces to the septic nonlinear Schrödinger equation:

$$iu_t + au_{xx} + b_3|u|^6u = 0. \tag{6.9}$$

This equation admits an exact bright soliton solution given by:

$$u(x,t) = A\,\mathrm{sech}^{\frac{1}{3}}\left[B(x - x_0 - 2akt)\right]e^{i(kx-\omega t)}, \tag{6.10}$$

where k is the wavenumber and ω is the frequency. These physical parameters must satisfy the following constraints:

$$B = \frac{3}{2}A^3\sqrt{\frac{b_3}{a}}, \quad \omega = ak^2 - \frac{1}{4}b_3A^6. \tag{6.11a}$$

For bright solitons to exist, the dispersion coefficient a and the nonlinearity coefficient b_3 must satisfy the focusing condition $ab_3 > 0$.

Now for the following exact solution:

$$u_{\text{exact}}(x,t) = A\,\mathrm{sech}^{\frac{1}{3}}\left[\frac{3}{2}A^3\sqrt{\frac{b_3}{a}}(x - x_0 - 2akt)\right]e^{i(kx-\left(ak^2-\frac{1}{4}b_3A^6\right)t)}, \tag{6.12}$$

we select the following constants:

$$a = b_3 = 1, \quad A = 1.0, \quad k = 1.0, \quad \omega = 0.75, \quad B = 1.5 \tag{6.13}$$

for our first numerical experiments. Additionally, we set the initial soliton center to $x_0 = -20$. The algorithm is initialized using the condition obtained by evaluating Eq (6.12) at $t = 0$.

We now proceed to investigate the computational accuracy and convergence properties of the proposed scheme with respect to both temporal and spatial variables at a final time of $T = 5$ and $x \in [-40, 40]$. The numerical results are summarized in Tables 1 and 2. In the spatial convergence test in Table 1, we utilized a scaling of $\tau = h^2$ to ensure that the temporal error does not dominate. The resulting data clearly demonstrate that the convergence rates $r_{h,2}$ and $r_{h,\infty}$ approach 4.0, indicating that the proposed scheme given by Eqs (3.10a)–(3.10c) and (3.12) achieves fourth-order accuracy in

space. Conversely, Table 2 fixes the spatial parameters to isolate the temporal error, and the computed rates asymptotically approach 2.0, confirming that the scheme is second-order accurate in time.

Table 1. Spatial errors and convergence rates of the present scheme when $h = 1/4, \tau = h^2, T = 5$.

h	$\|e^n\|_2$	$r_{h,2}$	$\|e^n\|_\infty$	$r_{h,\infty}$
1/4	6.5511×10^{-1}	\	5.4588×10^{-1}	\
1/8	2.6597×10^{-2}	4.6224	1.9136×10^{-2}	4.8342
1/16	1.6382×10^{-3}	4.0211	1.1723×10^{-3}	4.0289
1/32	1.0240×10^{-4}	3.9999	7.3258×10^{-5}	4.0002
1/64	6.4138×10^{-6}	3.9968	4.5674×10^{-6}	4.0035

Table 2. Temporal errors and convergence rates of the present scheme when $h = \tau = 1/16, T = 5$.

τ	$\|e^n\|_2$	$r_{\tau,2}$	$\|e^n\|_\infty$	$r_{\tau,\infty}$
1/16	3.1066×10^{-1}	\	2.3850×10^{-1}	\
1/32	6.4216×10^{-2}	2.2743	4.6444×10^{-2}	2.3604
1/64	1.5414×10^{-2}	2.0587	1.1023×10^{-2}	2.0750
1/128	3.8157×10^{-3}	2.0142	2.7214×10^{-3}	2.0181
1/256	9.5160×10^{-4}	2.0035	6.7821×10^{-4}	2.0045

We perform a comparative analysis between the exact solitary wave solutions and their numerical approximations at the different time instances $T \in \{1, 4, 8, 12, 15\}$, and the results are illustrated in Figure 1. The numerical simulations are conducted on the domain $\Omega = [-40, 40]$ using the discretization parameters $h = 0.01$ and $\tau = 0.0001$. Furthermore, we monitor the discrete invariants M^n and E^n to validate the conservation properties established in Propositions 4.1 and 4.2. The evolution of these conserved quantities is presented in Figure 2.

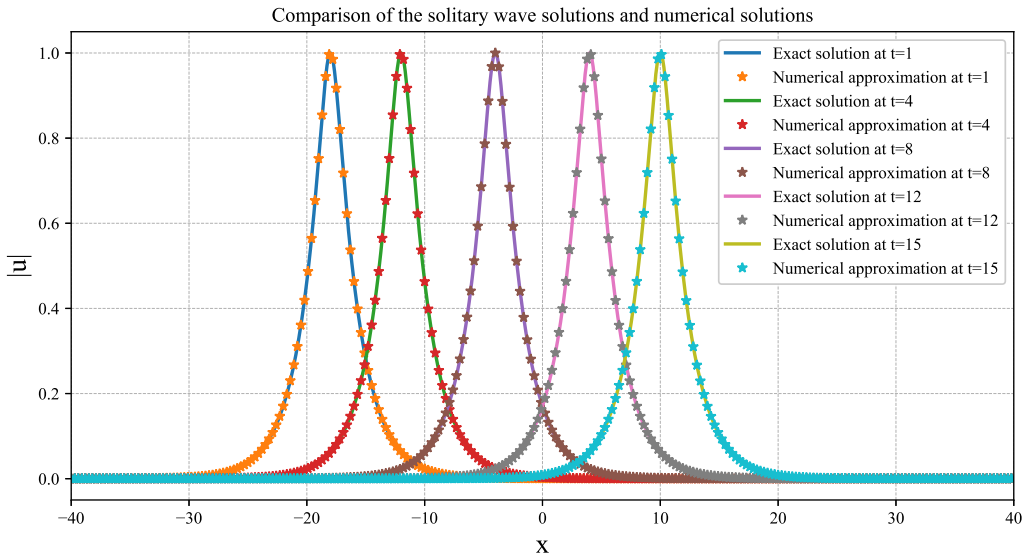

Figure 1. Comparison of the exact solitary wave solutions Eq (6.12) and the numerical approximations at various time instances $T = 1, 4, 8, 12, 15$ for Eq (6.9).

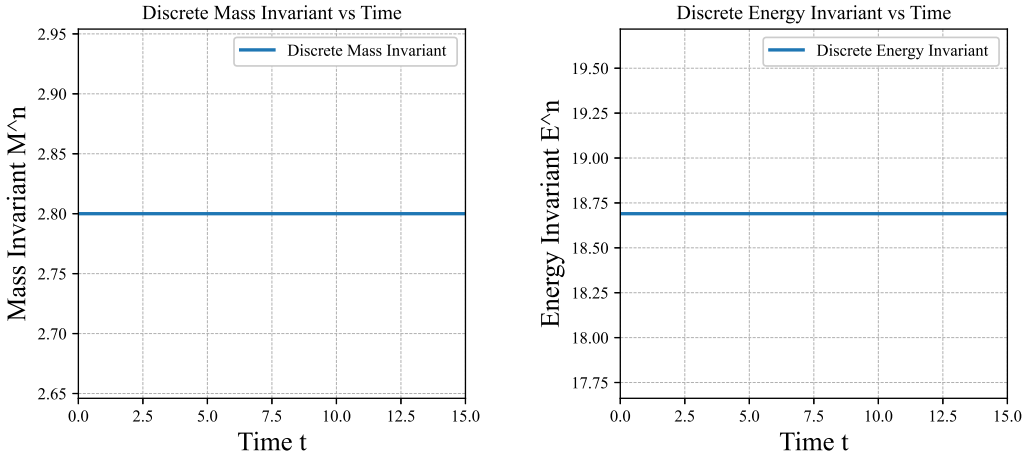

Figure 2. Time evolution of the discrete mass M^n and energy E^n invariants for Eq (6.9).

6.4. Example 2

We now turn our attention to the quintic reduction of the generalized equation, which is physically significant, as the quintic nonlinear Schrödinger equation frequently arises in the modeling of double-doped optical fibers and dense nonlinear media. Testing this reduction ensures that our numerical method maintains its high-order accuracy and conservation properties across different regimes of nonlinearity.

By setting $b_1 = b_3 = 0$, the governing equation simplifies to:

$$iu_t + au_{xx} + b_2|u|^4u = 0. \tag{6.14}$$

This equation admits an exact bright soliton solution with a profile distinct from the septic case, given

by:

$$u(x,t) = A\,\mathrm{sech}^{\frac{1}{2}}\left(B(x-2akt)\right)e^{i(kx-\omega t)} \tag{6.15}$$

where k is the wavenumber and ω is the frequency. These physical parameters must satisfy the following constraints:

$$A = \left[\frac{3(ak^2-\omega)}{b_2}\right]^{1/4}, \quad B = 2\sqrt{\frac{ak^2-\omega}{a}}. \tag{6.16}$$

For this numerical experiment, we select the physical parameters:

$$a = 1, \quad b_2 = 1, \quad k = 1, \quad \omega = 0.5. \tag{6.17}$$

The simulation is initialized using the exact solution at $t = 0$, centered at $x_0 = -10$, on the computational domain $\Omega = [-40, 40]$ with a final time of $T = 5$.

The accuracy and convergence properties are assessed using the same methodology as in Example 1. The results are tabulated in Tables 3 and 4. In Table 3, where we imposed the scaling $\tau = h^2$ to suppress temporal errors, the scheme exhibits a clear fourth-order spatial convergence rate. Conversely, when the spatial mesh is fixed to isolate temporal discretization errors, the convergence rates asymptotically approach 2.0 as shown in Table 4. These results confirm that the proposed conservative scheme maintains its $O(\tau^2 + h^4)$ accuracy regardless of the specific nonlinearity power.

Table 3. Spatial errors and convergence rates of the present scheme when $h = 1/4, \tau = h^2, T = 5$.

h	$\|\|e^n\|\|_2$	$r_{h,2}$	$\|\|e^n\|\|_\infty$	$r_{h,\infty}$
1/4	2.0359×10^{-1}	\	1.3822×10^{-1}	\
1/8	1.1723×10^{-2}	4.1182	7.8498×10^{-3}	4.1381
1/16	7.3345×10^{-4}	3.9985	4.9083×10^{-4}	3.9994
1/32	4.5903×10^{-5}	3.9980	3.0722×10^{-5}	3.9979
1/64	6.4138×10^{-6}	3.9345	4.5674×10^{-6}	4.0097

Table 4. Temporal errors and convergence rates of the present scheme when $h = \tau = 1/16, T = 5$.

τ	$\|\|e^n\|\|_2$	$r_{\tau,2}$	$\|\|e^n\|\|_\infty$	$r_{\tau,\infty}$
1/16	9.2392×10^{-2}	\	5.6063×10^{-2}	\
1/32	2.0671×10^{-2}	2.1601	1.2233×10^{-2}	2.1963
1/64	5.0268×10^{-3}	2.0399	2.9555×10^{-3}	2.0493
1/128	1.2480×10^{-3}	2.0100	7.3251×10^{-4}	2.0125
1/256	3.1144×10^{-4}	2.0026	1.8271×10^{-4}	2.0033

A visual comparison between the numerical approximation and the analytical solution is provided in Figure 3 for time instances $T \in \{1, 4, 8, 12, 15\}$. The profiles are indistinguishable, indicating that the soliton propagates without phase lag or amplitude distortion. Finally, the discrete mass M^n and energy E^n are plotted in Figure 4.

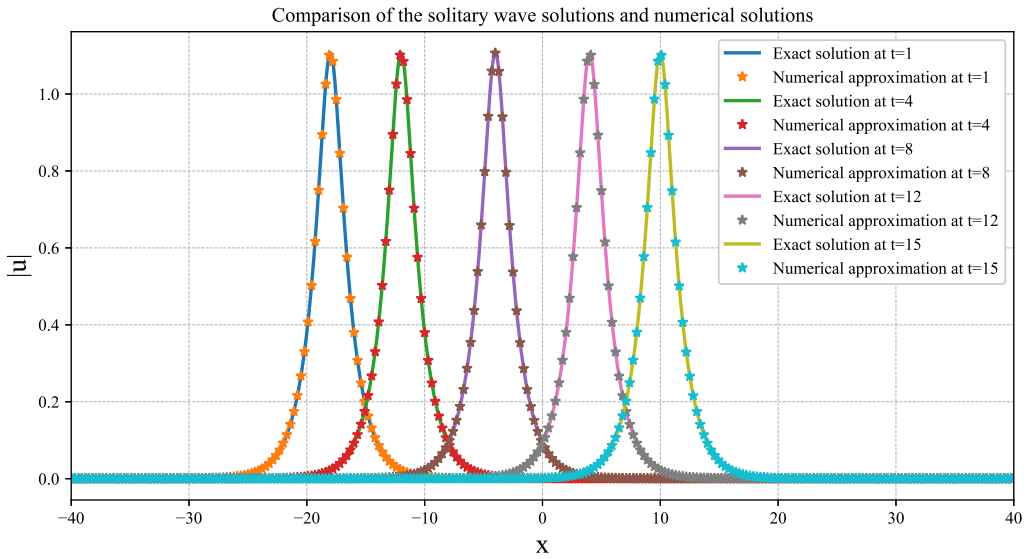

Figure 3. Comparison of the exact solitary wave solutions Eq (6.15) and the numerical approximations at various time instances $T = 1, 4, 8, 12, 15$ for Eq (6.14).

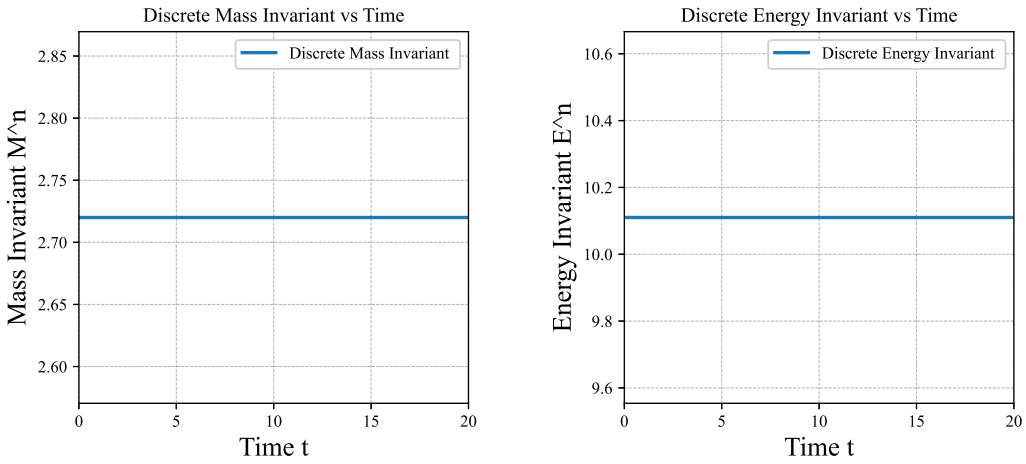

Figure 4. Time evolution of the discrete mass M^n and energy E^n invariants for Eq (6.15).

6.5. Example 3

In our third numerical experiment, we consider the fully generalized nonlinear Schrödinger equation where all nonlinearity coefficients are non-zero. In this regime, simple closed-form analytical solutions are generally intractable. Consequently, this test case is used to demonstrate the robustness of the scheme in simulating complex wave dynamics where the exact profile is unknown, and to validate the conservation properties in a physically general setting.

We simulate the interaction of competing nonlinearities by selecting the following parameters:

$$a = 1.0, \quad b_1 = 0.5, \quad b_2 = -0.5, \quad b_3 = 0.1. \tag{6.18}$$

To test the scheme's capability in handling complex arithmetic and wave transport, we impose a

complex-valued initial condition utilizing a Gaussian pulse:

$$u(x,0) = \exp\left(-\frac{1}{2}(x-x_0)^2 + 2i(x-x_0)\right). \tag{6.19}$$

The simulation was performed over the time interval $t \in [0, 12]$ on the spatial domain $\Omega = [-100.0, 100.0]$ and we set the initial center $x_0 = -30$.

At first, we evaluated the spatial accuracy via the Cauchy error analysis based on Eqs (6.7a), (6.7b), and (6.8). We computed the difference between the numerical solutions obtained on a coarse grid with mesh size h and a refined grid with mesh size $h/2$. Table 5 lists the L_2-norms and L_∞-norms of these errors at $T = 1$, alongside the corresponding convergence orders. Notably, the computed convergence rates asymptotically approach 4 in both norms.

Table 5. Spatial errors and convergence rates of the present scheme when $h = 1/4, \tau = 0.0001, T = 1$.

coarse h	fine h	$\|e^n\|_2$	$r_{h,2}$	$\|e^n\|_\infty$	$r_{h,\infty}$
1/4	1/8	2.6598×10^{-2}	\	1.4068×10^{-2}	\
1/8	1/16	1.7711×10^{-3}	3.9086	9.1727×10^{-4}	4.8342
1/16	1/32	1.1241×10^{-4}	3.9778	5.8127×10^{-5}	4.0289
1/32	1/64	7.0529×10^{-6}	3.9944	3.6461×10^{-6}	4.0002

Remark 6.1. *We only focus the Cauchy analysis on the spatial dimension to rigorously confirm the fourth-order convergence with order $O(h^4)$ of the proposed compact difference scheme. We omit the analogous temporal Cauchy test in this section, as the temporal accuracy has already been definitively established as $O(\tau^2)$ via the exact solution comparison in previous subsections.*

Unlike the previous examples, strictly exact energy conservation is not anticipated in this configuration, as the discrete energy invariant relies on Neumann boundary conditions that are not valid here. However, the discrete mass remains a robust invariant. The wave propagation profiles at selected time instances $t \in \{0, 4, 8, 12\}$ are illustrated in Figure 5, while the discrete mass is presented in Figure 6.

The numerical results presented in Figure 5 exhibit a distinct broadening of the wave packet accompanied by a monotonic decay in wave amplitude. This behavior is consistent with the physical governing dynamics of the generalized nonlinear Schrödinger equation for the selected parameters. Because the arbitrary complex Gaussian initial condition in Eq (6.19) lacks the precise phase-amplitude coupling required to form a stable soliton, the initial dispersive pressure (dominated by the term au_{xx}) is not perfectly balanced by the competing nonlinear self-focusing and defocusing effects. This imbalance leads to natural dispersive spreading, where the spectral components of the wave packet propagate at varying phase velocities, causing spatial delocalization.

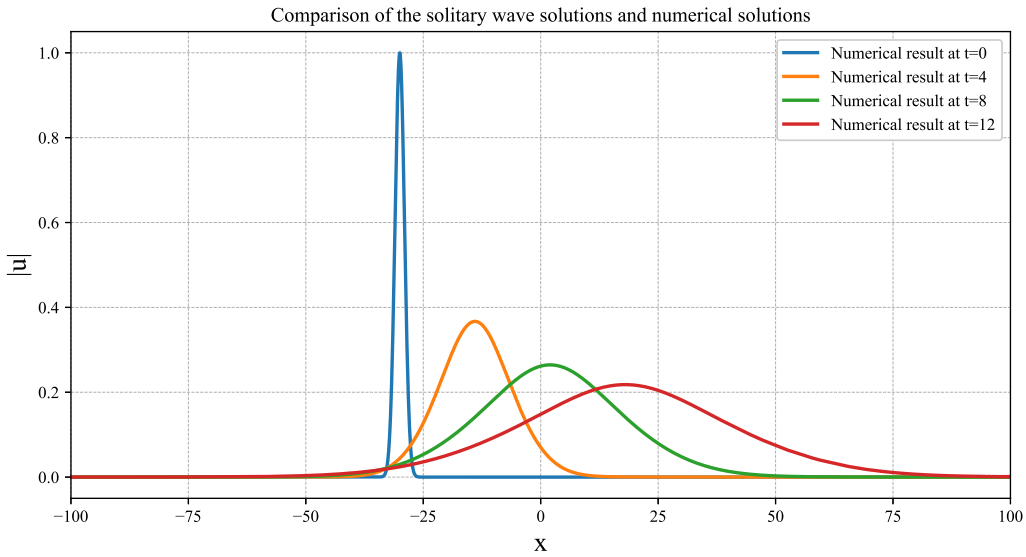

Figure 5. Evolution of the Gaussian wave for the general cubic-quintic-septic equation at $t = 0, 4, 8, 12$.

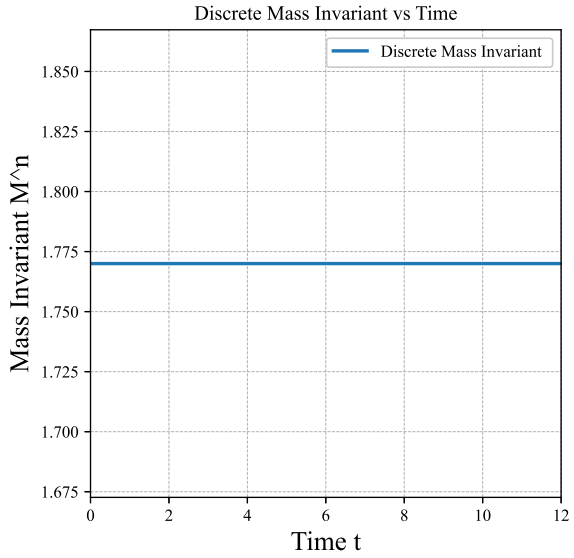

Figure 6. Time evolution of the discrete mass M^n over $t \in [0, 12]$.

Furthermore, the observed monotonic decay in amplitude is a direct physical consequence of the conservation of the mass invariant, which our numerical scheme strictly preserves (as shown in Figure 6). The mass constraint dictates an inverse relationship between the spatial width and the peak amplitude of the wave packet. As the packet broadens due to uncompensated dispersion, the maximum amplitude $\max_x |u(x,t)|$ must decrease proportionately to maintain a constant integrated power. Thus, the amplitude attenuation is a physical necessity governed by mass conservation rather than an artifact of numerical dissipation.

7. Conclusions

In this work, we have systematically investigated the nonlinear Schrödinger equation with cubic-quintic-septic nonlinearity. We verified the conservation of physical quantities, including mass, energy, and momentum, which are essential for the physical validity of the model. To solve this equation, we have developed a conservative finite difference scheme that achieves fourth-order accuracy in space and second-order accuracy in time.

We have established the discrete conservation laws for the proposed scheme and proved their consistency with the continuous energy and momentum laws. Through rigorous error analysis, we have proved the unconditional stability and convergence of the scheme, confirming a convergence rate of $O(\tau^2 + h^4)$. Numerical simulations, including septic and quintic reductions, confirmed the theoretical error bounds and demonstrated the scheme's ability to preserve discrete invariants over long-time simulations. The results indicate that the proposed method is an effective tool for studying high-order nonlinear wave phenomena.

An important feature for the model is that the paper tacitly ignored the aspect of soliton radiation. It can only be explored with additional mathematical approaches such as the implementation of the variational principle, beyond-all-order asymptotics, or even the inverse scattering transform. Such studies are reserved for the future. We also plan to extend the current method to two-dimensional nonlinear Schrödinger equations, which are important for modeling beam propagation in bulk media. Additionally, we intend to investigate systems with gain/loss perturbation terms, which would allow our conservative scheme to be adapted for modeling dissipative solitons in fiber lasers with amplifiers.

Author contributions

Conceptualization, Jiaqi Chen and Weizhong Dai; methodology, Weizhong Dai and Anjan Biswas; validation, Jiaqi Chen; formal analysis, Jiaqi Chen; writing–original draft preparation, Jiaqi Chen; writing–review and editing, Jiaqi Chen and Weizhong Dai; supervision, Weizhong Dai and Anjan Biswas. All authors have read and agreed to the published version of the manuscript.

Use of Generative-AI tools declaration

The authors declare they have not used Artificial Intelligence (AI) tools in the creation of this paper.

Acknowledgments

Jiaqi Chen is partially supported by the Scientific Research Foundation of Xiamen University of Technology under grant (No. YKJ23009R), the Scientific Research Foundation for Young and Middle Aged Teachers in Fujian Province under grant (No. JAT231105). The last author, A. Biswas, is supported by the funds of the Endowed Chair at Grambling State University and this support is gratefully acknowledged.

Conflict of interest

All authors declare no conflicts of interest in this paper.

References

1. G. Agrawal, *Fiber-optic communication systems*, John Wiley & Sons, 2010. https://doi.org/10.1002/9780470918524
2. N. Akhmediev, A. Ankiewicz, *Solitons: Nonlinear pulses and beams*, New York: Springer, 1997.
3. T. Cazenave, *Semilinear Schrödinger equations*, American Mathematical Society, 2003.
4. A. Wazwaz, L. Kaur, Optical solitons for nonlinear Schrödinger (NLS) equation in normal dispersive regimes, *Optik*, **184** (2019), 428–435. https://doi.org/10.1016/j.ijleo.2019.04.118
5. N. Kudryashov, Families of nonlinear Schrödinger equations in general form with exact solutions, *Phys. Lett. A*, **552** (2025), 130648. https://doi.org/10.1016/j.physleta.2025.130648
6. N. Kudryashov, A. Polyanin, Nonlinear Schrödinger equations of general form and their exact solutions, *Appl. Math. Lett.*, **170** (2025), 109622. https://doi.org/10.1016/j.aml.2025.109622
7. A. Biswas, Optical soliton cooling with polynomial law of nonlinear refractive index, *J. Opt.*, **49** (2020), 580–583. https://doi.org/10.1007/s12596-020-00644-0
8. N. Akhmediev, A. Ankiewicz, R. Grimshaw, Hamiltonian-versus-energy diagrams in soliton theory, *Phys. Rev. E*, **59** (1999), 6088. https://doi.org/10.1103/physreve.59.6088
9. R. Shohib, M. Alngar, A. Arnous, A. Biswas, B. Rawal, Y. Yildirim, et al., Optical soliton parameters by variational principle: Polynomial and triple power-laws (super-Gaussian and super-sech pulses), *Ukr. J. Phys. Opt.*, **25** (2024), 03068–03092. https://doi.org/10.3116/16091833/Ukr.J.Phys.Opt.2024.03068
10. D. Wang, Z. Liu, H. Zhao, H. Qin, G. Bai, C. Chen, et al., Launching by cavitation, *Science*, **389** (2025), 935–939. https://doi.org/10.1126/science.adu8943
11. Z. Si, D. Wang, B. Zhu, Z. Ju, X. Wang, W. Liu, et al., Deep learning for dynamic modeling and coded information storage of vector-soliton pulsations in mode-locked fiber lasers, *Laser Photonics Rev.*, **18** (2024), 2400097. https://doi.org/10.1002/lpor.202400097
12. Z. Si, Z. Ju, L. Ren, X. Wang, B. Malomed, C. Dai, Polarization-induced buildup and switching mechanisms for soliton molecules composed of noise-like-pulse transition states, *Laser Photonics Rev.*, **19** (2025), 2401019. https://doi.org/10.1002/lpor.202401019
13. I. Mendez Zuniga, T. Belyaeva, M. Agüero, V. Serkin, Multisoliton bound states in the fourth-order concatenation model of the nonlinear Schrödinger equation hierarchy, *Trans. Opt. Photonics*, 2026, 22–33.
14. D. Mou, Z. Si, W. Qiu, C. Dai, Optical soliton formation and dynamic characteristics in photonic Moiré lattices, *Opt. Laser Technol.*, **181** (2025), 111774. https://doi.org/10.1016/j.optlastec.2024.111774
15. T. Belyaeva, L. Kovachev, V. Serkin, Parton-like soliton structures in nonlinear coherent states, *Optik*, **210** (2020), 164483. https://doi.org/10.1016/j.ijleo.2020.164483

16. J. Yang, Y. Zhu, W. Qin, S. Wang, C. Dai, J. Li, Higher-dimensional soliton structures of a variable-coefficient Gross-Pitaevskii equation with the partially nonlocal nonlinearity under a harmonic potential, *Nonlinear Dyn.*, **108** (2022), 2551–2562. https://doi.org/10.1007/s11071-022-07337-2
17. J. Yang, Y. Zhu, W. Qin, S. Wang, J. Li, 3D bright-bright Peregrine triple-one structures in a nonautonomous partially nonlocal vector nonlinear Schrödinger model under a harmonic potential, *Nonlinear Dyn.*, **111** (2023), 13287–13296. https://doi.org/10.1007/s11071-023-08526-3
18. K. Omar, F. Easif, Numerical solution of cubic-quintic nonlinear Schrödinger equation, *Sci. J. Univ. Zakho*, **13** (2025), 499–509. https://doi.org/10.25271/sjuoz.2025.13.4.1595
19. H. Ibarra Villalon, O. Pottiez, A. Gómez Vieyra, J. Lauterio Cruz, Comparative study of finite difference methods and pseudo-spectral methods for solving the nonlinear Schrödinger equation in optical fiber, *Phys. Scr.*, **98** (2023), 065514. https://doi.org/10.1088/1402-4896/acd22c
20. Z. Z. Sun, *Numerical solution methods for partial differential equations (in Chinese)*, Beijing: Science Press, 2005.
21. X. Wang, An energy-preserving finite difference scheme with fourth-order accuracy for the generalized Camassa-Holm equation, *Commun. Nonlinear Sci. Numer. Simul.*, **119** (2023), 107–121. https://doi.org/10.1016/j.cnsns.2023.107121
22. W. Dai, R. Nassar, A finite difference scheme for the generalized nonlinear Schrödinger equation with variable coefficients, *J. Comput. Math.*, **18** (2000), 123–132.
23. M. Delfour, M. Fortin, G. Payr, Finite-difference solutions of a non-linear Schrödinger equation, *J. Comput. Phys.*, **44** (1981), 277–288. https://doi.org/10.1016/0021-9991(81)90052-8
24. X. Wang, W. Dai, A. Biswas, A conservative higher-order finite difference scheme for solving the Gardner equation with dual power-law nonlinearities in both 1D and 2D, *Comput. Math. Appl.*, **201** (2026), 171–194. https://doi.org/10.1016/j.camwa.2025.10.023
25. L. Evans, *Partial differential equations*, American Mathematical Society, 2010.
26. X. Wang, H. Cheng, Solitary wave solution and a linear mass-conservative difference scheme for the generalized Korteweg-de Vries-Kawahara equation, *Comput. Appl. Math.*, **40** (2021), 273. https://doi.org/10.1007/s40314-021-01668-3
27. N. Tamang, B. Wongsaijai, T. Mouktonglang, K. Poochinapan, Novel algorithm based on modification of Galerkin finite element method to general Rosenau-RLW equation in (2+1)-dimensions, *Appl. Numer. Math.*, **148** (2020), 109–130. https://doi.org/10.1016/j.apnum.2019.07.021

AIMS Press